Please cite this article in press as: Kallen et al., The Imprinted H19 LncRNA Antagonizes Let-7 MicroRNAs, Molecular Cell (2013), http://dx.doi.org/10.1016/j.molcel.2013.08.027

Molecular Cell
Article

The Imprinted H19 LncRNA Antagonizes Let-7 MicroRNAs

Amanda N. Kallen,[1,11] Xiao-Bo Zhou,[1,5,11] Jie Xu,[1,12] Chong Qiao,[1,6] Jing Ma,[1,7] Lei Yan,[1,8] Lingeng Lu,[2] Chaochun Liu,[9] Jae-Sung Yi,[3] Haifeng Zhang,[4] Wang Min,[4] Anton M. Bennett,[3] Richard I. Gregory,[10] Ye Ding,[9] and Yingqun Huang[1,*]
[1]Department of Obstetrics, Gynecology and Reproductive Sciences, Yale Stem Cell Center
[2]Department of Chronic Diseases Epidemiology, Yale School of Public Health
[3]Department of Pharmacology
[4]Department of Pathology
Yale University School of Medicine, New Haven, CT 06510, USA
[5]Department of Immunology and Pathogenic Biology, School of Medicine, Xi'an Jiaotong University, Xi'an, Shaanxi 710061, P.R. China
[6]Department of Obstetrics and Gynecology, Shengjing Hospital, China Medical University, Shengyang, Liaoning 110004, P.R. China
[7]Obstetrics and Gynecology Department, Third Xiangya Hospital of Central South University, Changsha, Hunan 410013, P.R. China
[8]Department of Obstetrics and Gynecology, Provincial Hospital affiliated to Shandong University, Jinan, Shandong 250021, P.R. China
[9]Laboratory of Computational & Structural Biology, Division of Genetics, Wadsworth Center, New York State Department of Health, 150 New Scotland Avenue, Albany, NY 12208, USA
[10]Stem Cell Program, Children's Hospital Boston, and Biological Chemistry & Molecular Pharmacology, Harvard Medical School, Boston, MA 02115, USA
[11]These authors contributed equally to this work
[12]Present address: Institute of Cancer Stem Cell, Dalian Medical University, Dalian, Liaoning 116044, P.R. China
*Correspondence: yingqun.huang@yale.edu
http://dx.doi.org/10.1016/j.molcel.2013.08.027

SUMMARY

Abundantly expressed in fetal tissues and adult muscle, the developmentally regulated H19 long noncoding RNA (lncRNA) has been implicated in human genetic disorders and cancer. However, how H19 acts to regulate gene function has remained enigmatic, despite the recent implication of its encoded miR-675 in limiting placental growth. We noted that vertebrate H19 harbors both canonical and noncanonical binding sites for the let-7 family of microRNAs, which plays important roles in development, cancer, and metabolism. Using H19 knockdown and overexpression, combined with in vivo crosslinking and genome-wide transcriptome analysis, we demonstrate that H19 modulates let-7 availability by acting as a molecular sponge. The physiological significance of this interaction is highlighted in cultures in which H19 depletion causes precocious muscle differentiation, a phenotype recapitulated by let-7 overexpression. Our results reveal an unexpected mode of action of H19 and identify this lncRNA as an important regulator of the major let-7 family of microRNAs.

INTRODUCTION

The *H19* gene belongs to a highly conserved imprinted gene cluster that plays important roles in embryonal development and growth control (Gabory et al., 2010). The cluster also contains the nearby reciprocally imprinted gene for insulin-like growth factor 2 (*Igf2*), which is coordinately regulated by an intergenic control region and a common enhancer region. In human and mouse, *H19* is expressed from the maternal allele, while *Igf2* is paternally expressed. *H19* expression is strongly induced during embryogenesis and downregulated after birth, except in adult skeletal muscle and heart (Gabory et al., 2010; Onyango and Feinberg, 2011). Two human genetic disorders have been linked to the *H19-Igf2* locus: Silver-Russell syndrome and Beckwith-Wiedemann syndrome, with the latter also displaying higher susceptibility to the development of embryonal tumors (Gabory et al., 2010). Further, a role for *H19* acting either as a tumor suppressor (Yoshimizu et al., 2008) or an oncogene (Matouk et al., 2007) has been suggested. However, how *H19* functions to impact these various processes remains poorly understood.

The human *H19* encodes a predominantly cytoplasmic ~2.3 kb long, capped, spliced, and polyadenylated RNA that produces no known protein product (Brannan et al., 1990). In the past two decades, extensive investigations using both deletion and transgenic mouse models have yielded important insights into the functional role of *H19* (Gabory et al., 2010). It has been reported that mice with targeted *H19* deletion (*H19Δ3*) exhibit an overgrowth phenotype (an increase in postnatal growth by 8% compared to wild-type [WT] littermates), which was restored to WT growth by transgenic expression of *H19* (Gabory et al., 2009). Importantly, overexpression of several genes of the imprinted gene network (IGN) (Varrault et al., 2006), including *Igf2* in the *H19Δ3* mice, was concomitantly restored to the WT level by such transgenic expression. This suggests that the H19 long noncoding RNA (lncRNA) acts in *trans* to regulate the IGN and control growth in mice (Gabory et al., 2009). However, the mechanism by which H19 does so is unclear. Recently, a role for *H19* in limiting placental growth through its encoded miR-675 has been reported (Keniry et al., 2012). This microRNA (miRNA) is produced from full-length H19 through

Please cite this article in press as: Kallen et al., The Imprinted H19 LncRNA Antagonizes Let-7 MicroRNAs, Molecular Cell (2013), http://dx.doi.org/10.1016/j.molcel.2013.08.027

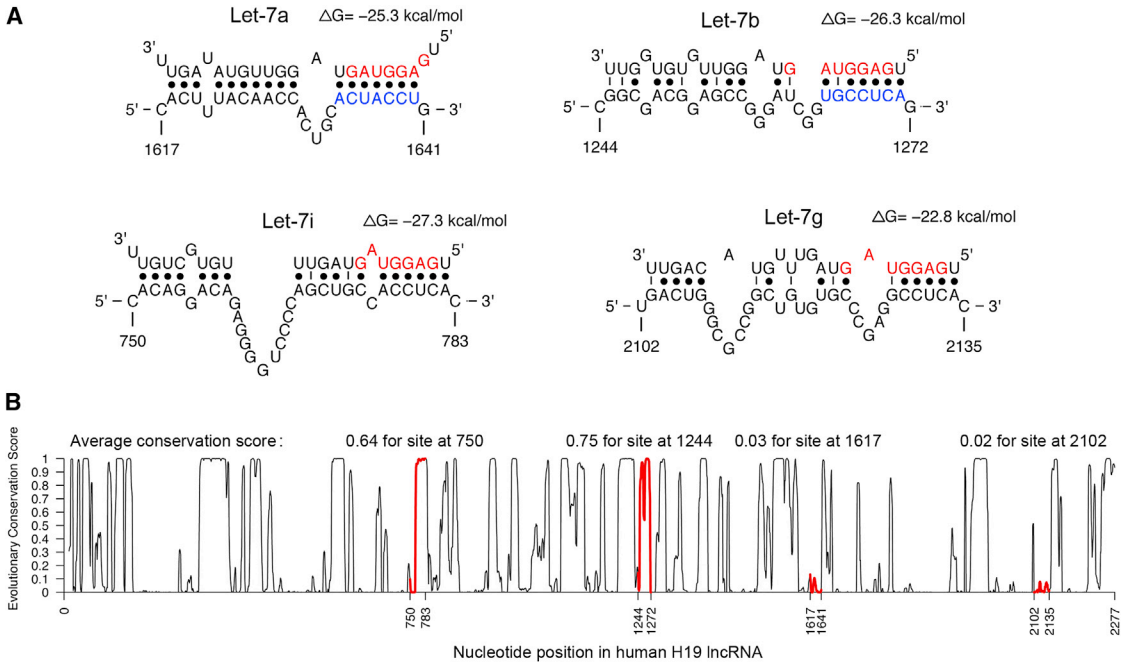

Figure 1. Bioinformatics Predicted Let-7 Binding Sites at Four Distinct Positions in Human H19

(A) Partial sequences of H19 and sequences of four let-7 subtypes are shown. Nucleotides of the miRNA seed region (positions 2–8) are in red. Numbers are in nucleotides relative to the transcriptional start site of H19. The deleted nucleotides in psiCHECK2-H19D are marked in blue. See also Figure S2A.

(B) Profile of evolutionary conservation scores for human H19 lncRNA. The portions of the profile for four let-7 binding sites are in red, with average conservation score given on top.

Drosha processing, and the miRNA is detected only in the mouse placenta and at a time window during which placental growth normally ceases (Keniry et al., 2012). Finally, high H19 expression has been detected in adult skeletal muscle of both human and mouse (Gabory et al., 2010; Onyango and Feinberg, 2011), but the physiological significance of this expression remains to be investigated. In the current study, we demonstrate that the H19 lncRNA acts as a molecular sponge for the major let-7 family of miRNAs, which are known to play important roles in diverse physiological and pathological processes.

RESULTS

H19 Contains Potential Let-7 Binding Sites

While in the process of defining the molecular function of H19, we unexpectedly noticed increased levels of the miRNA-processing enzyme Dicer in response to ectopic H19 expression in multiple cell types. Given that Dicer is a known target of let-7 (Forman et al., 2008; Tokumaru et al., 2008) and that lncRNAs can act as sponges to bind specific miRNAs and regulate their function (Ebert and Sharp, 2010; Salmena et al., 2011), we suspected that H19 might bind let-7 and interfere with its function. Let-7 regulates target gene expression by binding to imperfectly complementary sequences in messenger RNAs (mRNAs), leading to translational repression and/or mRNA destabilization (Fabian and Sonenberg, 2012). Subsequent bioinformatic analysis revealed putative complementary sequences for let-7 in human H19 (Figure 1A). Among the four predicted let-7 sites in human H19, the site with starting nucleotide at position 1,617 is an offset 6-mer seed site with strong compensatory base-pairing for the 3′ end of let-7 (Bartel, 2009). The other three sites are noncanonical (seedless) sites. However, the site at position 1,244 has strong base-paring in the seed region despite involving a G:U pair. From conservation analysis (based on sequence alignments of 33 mammalian genomes), we found that the conservation for human H19 varies greatly from region to region. After defining a conservation score threshold of 0.57 (Siepel et al., 2005), the sites at positions 1,244 and 750 are well and moderately conserved, with average conservation scores of 0.75 and 0.64, respectively. The sites at positions 1,617 and 2,102 are poorly conserved, with average conservation scores of 0.03 and 0.02, respectively (Figure 1B). The experimental results below for the site at position 1,244 are consistent with previous reports that noncanonical sites can be functional (Didiano and Hobert, 2006; Lal et al., 2009; Landthaler et al., 2008; Tay et al., 2008; Vella et al., 2004). This is further supported by the observation of large numbers of noncanonical sites identified by genome-wide RNA-binding protein immunoprecipitation microarray (RIP-Chip) and crosslinking immunoprecipitation-high-throughput sequencing (CLIP-seq) studies (Chi et al., 2009; Hafner et al., 2010; Landthaler et al., 2008). The findings on the seed site at position 1,617 suggest that there may be many more functional nonconserved seed sites than are currently known, as nonconserved seed sites outnumber conserved seed sites by about one order of magnitude (Bartel, 2009). Experiments described in Figure 2 suggest that both canonical and noncanonical sites can function in target regulation.

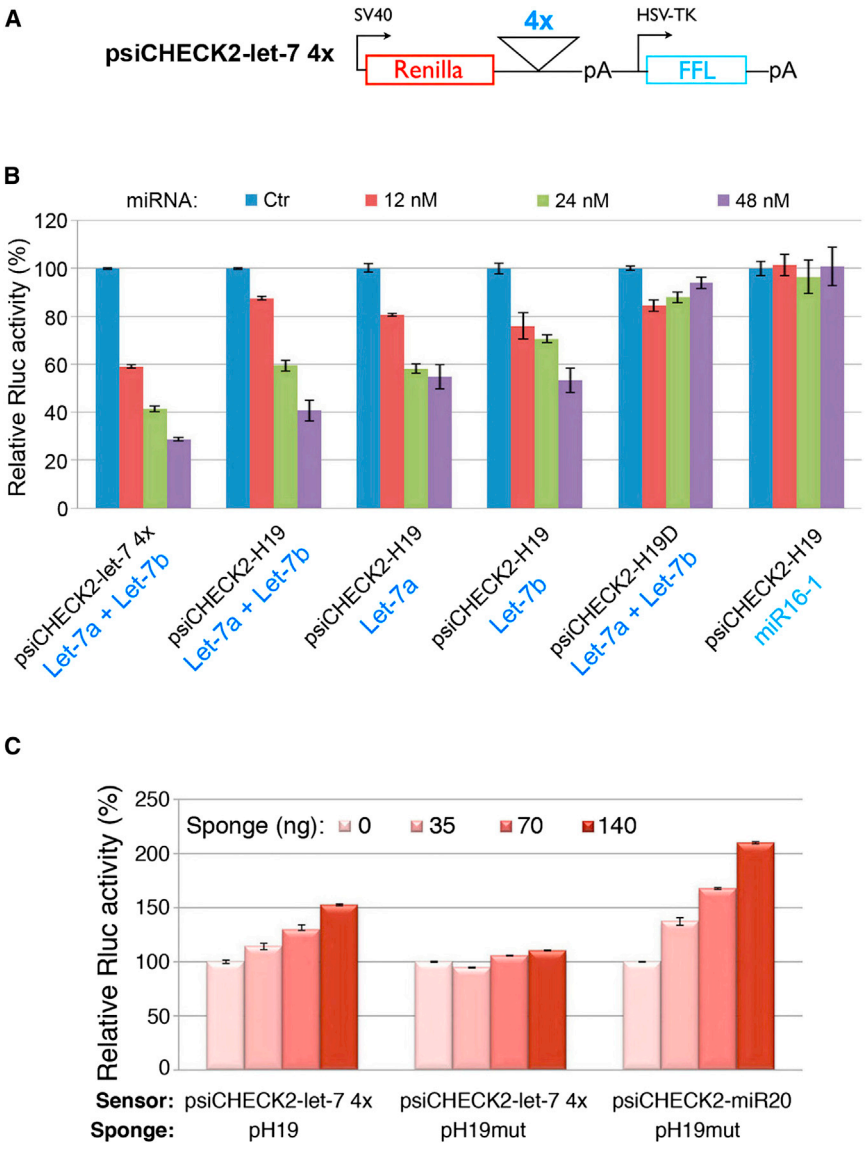

Figure 2. H19 Contains Functional Let-7 Interaction Sites

(A) Reporter constructs.

(B) The indicated constructs were each transfected into HEK 293 cells, together with control miRNA (Ctr), let-7, or miR-16-1 at a final concentration of 12, 24, or 48 nM. In Let-7a + Let-7b, equal concentrations of let-7a and let-7b were combined to give the indicated final concentrations. Numbers are mean ± SD (n = 3). See also Figure S1.

(C) Let-7 sensor (psiCHECK2-let-7 4x) or miR-20 sensor (psiCHECK2-miR-20) were transfected into HEK 293 cells, together with 0, 35, 70, or 140 ng of sponge plasmid pH19 or pH19mut. Numbers are mean ± SD (n = 3). See also Figures S2B and S3A.

The Let-7-Binding Sites Are Functional

Experiments using let-7 biosensors were carried out to determine the functionality of two predicted let-7 binding sites: positions 1,244 and 1,617. psiCHECK2-let-7 4x (Iwasaki et al., 2009) harbors four copies of let-7 binding sites (called 4x hereafter) in the 3′ UTR of a *Renilla luciferase* (*Rluc*) gene (Figure 2A). This plasmid also contains a downstream constitutively expressed firefly luciferase gene as an internal control for normalization. As expected, cotransfected let-7 inhibited Rluc expression in a dose-dependent manner (Figure 2B, first column from left). A dose-dependent inhibition was also observed with psiCHECK2-H19 containing a human H19 fragment at the 3′ UTR of the Rluc in place of 4x (Figure 2B, second column from left). This H19 fragment was predicted to bind both let-7a and let-7b at positions 1,244 and 1,617, respectively (Figure 1A). The extent of inhibition with psiCHECK2-H19 was slightly lower than that with psiCHECK2-let-7 4x, likely due to fewer let-7 binding sites (2 versus 4). In metazoans, multiple sites for the same or different miRNAs are generally required for effective repression (Bartel, 2009; Filipowicz et al., 2008). When let-7a and let-7b were tested individually, dose-dependent inhibitions were evident as well (Figure 2B, third and fourth columns from left). To confirm that the observed inhibition was dependent on the predicted let-7 sites, we tested psiCHECK2-H19D with deleted sequences complementary to the seed region of both let-7a and let-7b (Figure 1A, nucleotides marked in blue). This mutant no longer responded to let-7 inhibition in a dose-dependent manner (Figure 2B, second column from right). The slight repression seen at 12 nM and 24 nM might be results of let-7 3′ end interaction with H19 sequences. When miR-16-1 (not predicted to bind H19) was tested on psiCHECK2-H19, a dose-dependent inhibition was not observed (Figure 2B, first column from right). Together, these results suggest that positions 1,244 and 1,617 contain functional let-7 binding sites.

H19 Acts as a Molecular Sponge for Let-7

To determine whether H19 might act as a sponge to sequester let-7, we transfected psiCHECK2-let-7 4x (sensor) into human embryonic kidney (HEK) 293 cells, which do not express endogenous H19 but express appreciable levels of let-7 miRNAs (Figure S1A available online), together with increasing amounts of pH19 (sponge) that express full-length human H19. The Rluc activity increased in response to pH19 in a dose-dependent manner (Figure 2C, left column), suggesting that ectopically expressed H19 specifically sequestered endogenous let-7, thereby preventing it from inhibiting Rluc expression. To confirm whether let-7 binding sites are required for this effect, a mutant H19 (pH19mut), in which all four predicted let-7 interaction sites

Please cite this article in press as: Kallen et al., The Imprinted H19 LncRNA Antagonizes Let-7 MicroRNAs, Molecular Cell (2013), http://dx.doi.org/10.1016/j.molcel.2013.08.027

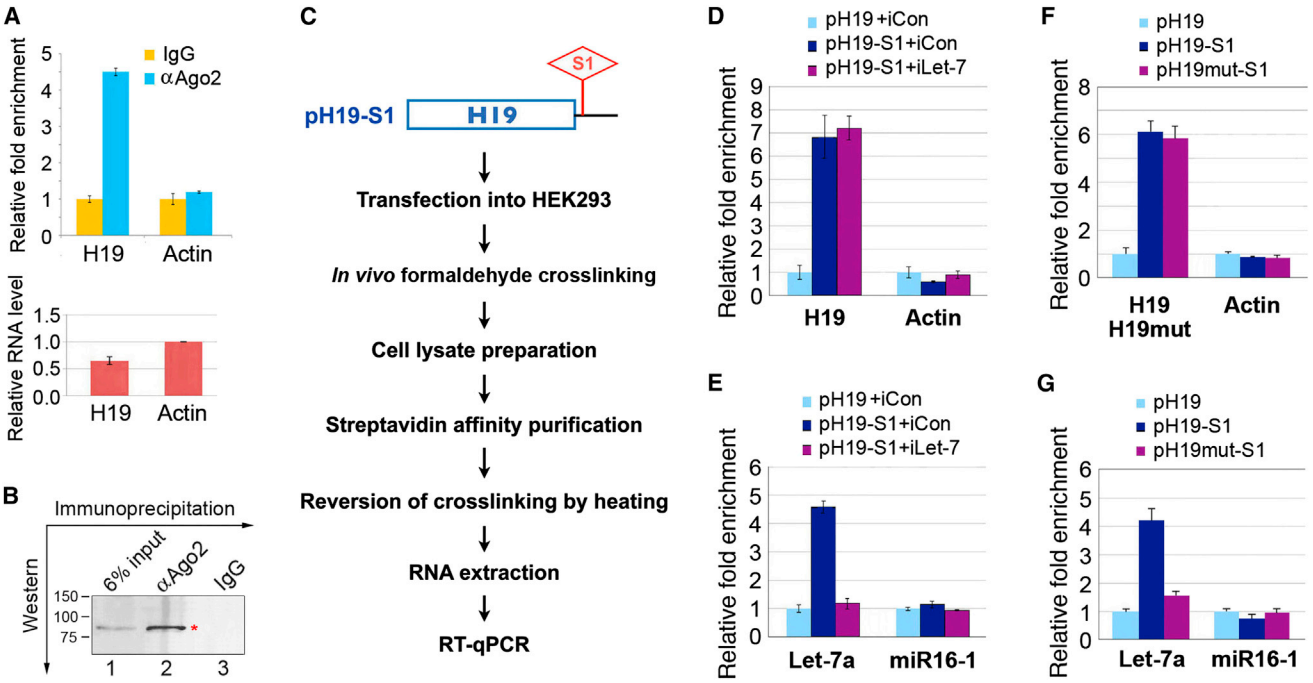

Figure 3. H19 Associates with miRNPs

(A) CoIP with mouse monoclonal anti-Ago2 (αAgo2) or preimmune IgG from extracts of retinoic acid (RA)-induced PA-1 cells. RNA levels in immunoprecipitates were determined by reverse transcription and quantitative real-time PCR (RT-qPCR). Top: levels of H19 and beta-actin RNA are presented as fold enrichment in αAgo2 relative to IgG immunoprecipitates. Bottom: relative RNA levels of H19 and beta-actin in RA-induced PA-1. Numbers are mean ± SD (n = 3).

(B) Immunoprecipitation using αAgo2 (lane 2) or IgG (lane 3) followed by western blot analysis using a rabbit monoclonal anti-Ago2. In lane 1, 6% input was loaded. The Ago2 band is marked with a red asterisk. Molecular markers in kDa are on the left.

(C) Schematic outline of purification of H19-associated RNPs and RNA component identification.

(D) pH19 (expressing untagged H19) or pH19-S1 (expressing S1-tagged H19) were transfected into HEK 293, with or without cotransfection of iCon or iLet-7. Cells were subjected to in vivo crosslinking followed by affinity purification of H19-associated RNPs. RNAs extracted from RNPs were subjected to RT-qPCR. Relative abundance of H19 and beta-actin RNA associated with tagged versus untagged H19 are plotted as relative fold enrichment after normalization against beta-tubulin mRNA levels. Numbers are mean ± SD (n = 3).

(E) Relative abundance of let-7a and miR-16-1 associated with tagged versus untagged H19 in RNPs purified as described in (D) are plotted as relative fold enrichment after normalization against U6B snRNA levels. Numbers are mean ± SD (n = 3).

(F) pH19, pH19-S1, or pH19mut-S1 (expressing S1-tagged mutant H19) were transfected into HEK 293. Cells were subjected to in vivo crosslinking followed by affinity purification of H19-associated RNPs. RNAs extracted from RNPs were subjected to RT-qPCR. Relative abundance of H19, muant H19 (H19mut), or beta-actin RNA associated with tagged versus untagged H19 are plotted as relative fold enrichment after normalization against beta-tubulin mRNA levels. Numbers are mean ± SD (n = 3).

(G) Relative abundance of let-7a and miR-16-1 associated with tagged versus untagged H19 in RNPs purified as described in (F) are plotted as relative fold enrichment after normalization against U6B snRNA levels. Numbers are mean ± SD (n = 3).

were mutated to sequences complementary to miR-20 (Figures S2A and S2B), was tested. Remarkably, this mutant no longer elicited such an effect (Figure 2C, middle column); rather, it gained an ability to derepress a miR-20 sensor (right column). Consistent with the absence of miR-20 sites in H19, dose-dependent derepression of psiCHECK2-miR-20 by pH19 was not observed (Figure S3A). Derepression of psiCHECK2-miR-20 by pH19mut was more efficient than that of psiCHECK2-let-7 4x by pH19, likely due to the fact that the miR-20 sites in pH19mut are much more complementary to miR-20 than the let-7 sites in pH19 are to let-7. Together, these results strongly point to a role of H19 as a molecular sponge for let-7.

H19 Associates with miRNPs

miRNAs are known to be present in the cytoplasm in the form of miRNA ribonucleoprotein complexes (miRNPs) that also contain Ago2, the core component of the RNA-induced silencing complex (RISC) (Filipowicz et al., 2008; Izaurralde, 2012). To test whether H19 associates with miRNPs, coimmunoprecipitation (coIP) experiments using antibodies against Ago2 on extracts of differentiating human embryonal carcinoma (EC) cell line PA-1 were carried out. H19 is expressed at low levels in undifferentiated embryonic stem cells (ESCs) and EC cells, but its expression is strongly upregulated during differentiation (Brannan et al., 1990; McKarney et al., 1996). H19 was preferentially enriched (~4.5-fold) in Ago2-containing miRNPs relative to control immunoglobulin G (IgG) immunoprecipitates (Figure 3A, top panel, left column, blue bar versus yellow bar), whereas beta-actin mRNA, expressed at a level ~1.5-fold greater than that of H19 (bottom panel), did not detectably associate with the miRNPs (top panel, right column). The specificity of the Ago2 antibody was confirmed by immunoprecipitation (IP) and

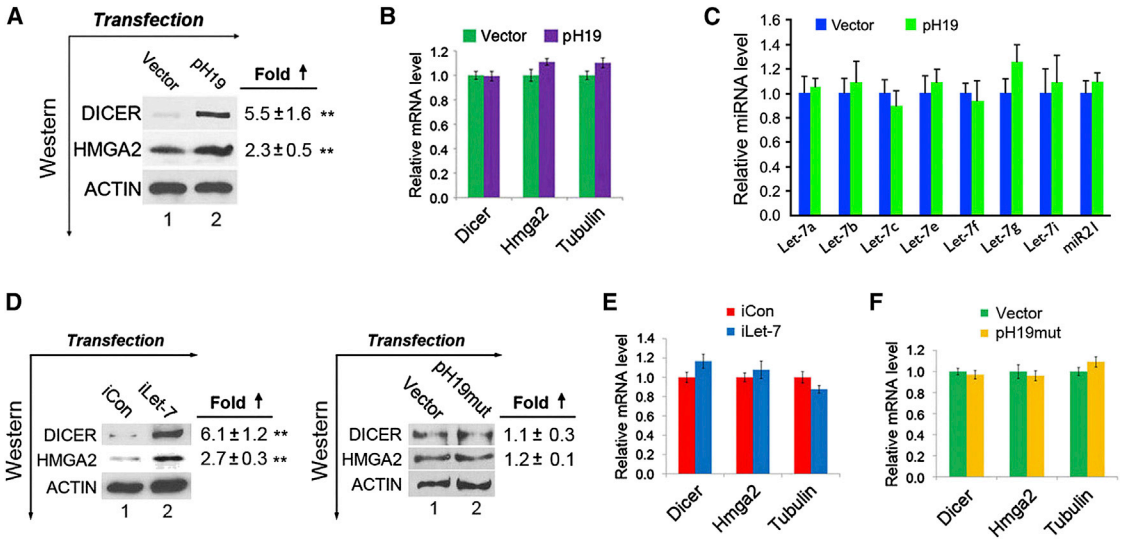

Figure 4. H19 Modulates Expression of Endogenous Let-7 Targets

(A–C) Empty vector or pH19 were transfected into HEK 293 cells. Protein and RNA were extracted 48 hr later, and levels were determined by western blot (A) and RT-qPCR (B and C). In (A), the fold increases in the protein levels relative to vector-transfected controls after normalization against beta-actin loading controls are marked on the right. Numbers are mean ± SD (n = 3); **p < 0.01. One-sample t tests were performed to compare each data point with the controls. See also Figure S1C. In (B), mRNA levels were normalized against those of beta-actin. Numbers are mean ± SD (n = 3). Group t tests were performed to compare means of each mRNA between vector- and pH19-transfected cells. See also Figure S1D. In (C), miRNA levels were normalized against those of U6B and presented as mean ± SD (n = 3). Group t tests were performed to compare means of each miRNA between vector- and pH19-transfected cells. See also Figure S1E.

(D) iCon, iLet-7, empty vector, or pH19mut were transfected into HEK 293 cells. Proteins were extracted 48 hr later, and levels were determined by western blot analysis. The fold increases in the protein levels relative to controls (iCon- or vector-transfected) after normalization against beta-actin loading controls are marked on the right. Numbers are mean ± SD (n = 3).

(E) RNAs were isolated from cells transfected with iCon or iLet-7 as described in (D). The levels of Dicer, Hmga2, and beta-tubulin mRNAs were determine by RT-qPCR and plotted after normalization against beta-actin mRNA levels. Numbers are mean ± SD (n = 3).

(F) RNAs were isolated from cells transfected with empty vector or pH19mut as described in (D). The levels of Dicer, Hmga2, and beta-tubulin mRNAs were determined by RT-qPCR and plotted after normalization against beta-actin mRNA levels. Numbers are mean ± SD (n = 3).

immunoblotting (Figure 3B). Selective H19 enrichment in miRNPs was also detected in HEK 293 cells ectopically expressing H19 (data not shown). Thus, H19 is present in Ago2-containing miRNPs, likely through association with let-7 and other miRNAs, as our bioinformatic analysis suggests that H19 contains putative binding sites for additional miRNAs (Table S1).

To further demonstrate the physical interaction between H19 and let-7, in vivo crosslinking combined with affinity purification experiments were carried out using an S1 aptamer-tagged H19 (pH19-S1) (Figure 3C). Thus, pH19-S1 (tagged) or pH19 (untagged) were transfected into HEK 293 cells, with or without cotransfection of let-7 inhibitor (iLet-7 or a control inhibitor iCon), followed by crosslinking and affinity purification of H19-associated ribonucleoprotein complexes (RNPs). RNAs were extracted from the RNPs and subjected to reverse transcription and real-time PCR (RT-qPCR) analysis. Effective affinity purification of tagged H19 RNPs was demonstrated by an ~7-fold preferential enrichment of the tagged versus untagged H19 in the purified RNPs (Figure 3D, left column, purple and dark blue bars versus light blue bar), while such an enrichment was not seen with beta-actin mRNA (right column). Let-7a was also preferentially enriched by ~5-fold in the tagged versus untagged H19 fraction (Figure 3E, left column, dark blue bar versus light blue bar). Importantly, the enrichment was abolished in the presence of iLet-7 (Figure 3E, left column, purple bar versus dark blue bar). No enrichment of miR-16-1 in tagged H19 was observed (right column). Crosslinking experiments using a tagged H19 mutant (pH19mut-S1) (Figures 3F and 3G) showed significantly reduced recovery of let-7 (Figure 3G, left column, purple bar versus dark blue bar). Together, these results strongly suggest that H19 physically interacts with let-7 in vivo and that functional let-7 sites are required for promoting this association.

H19 Affects Expression of Endogenous Let-7 Targets

To determine whether H19 affects the expression of endogenous let-7 targets, pH19 was transfected into HEK 293 cells, and the levels of expression of two known let-7 targets, Dicer (Forman et al., 2008; Tokumaru et al., 2008) and Hmga2 (Lee and Dutta, 2007), were analyzed. The transfected H19 was expressed at a level ~2.5-fold greater than that of beta-tubulin mRNA (Figure S1B, second column from left, red bar versus blue bar). A 5.5- and 2.3-fold increase in the protein level for DICER and HMGA2, respectively, in response to H19 expression was observed 48 hr posttransfection (Figure 4A), while the levels of the respective mRNAs were not changed (Figure 4B). miRNA-mediated repression generally involves translational repression followed by RNA degradation. However, examples of translational repression without RNA destabilization have also been documented (Filipowicz et al., 2008; Izaurralde, 2012). This apparent discrepancy is likely due to different cell types and/or

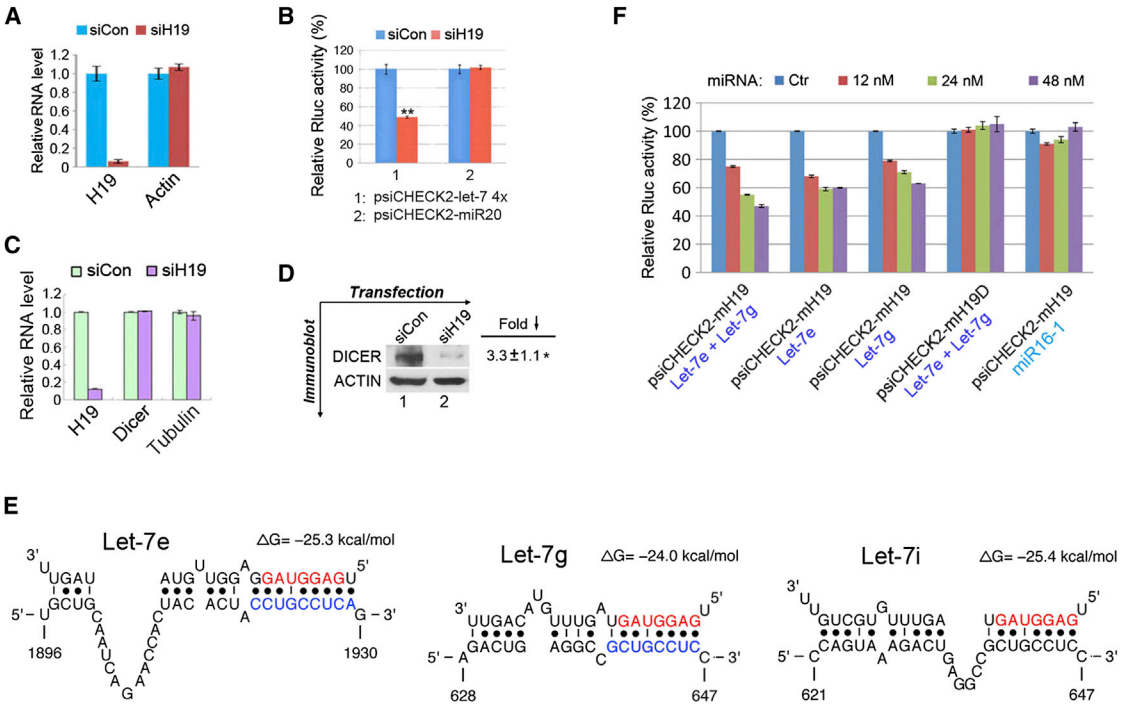

Figure 5. H19 Regulation of Let-7 Is Conserved

(A and B) PA-1 cells were RA induced to express endogenous H19, followed by siRNA transfection. Cells were subjected to a second transfection 48 hr later with psiCHECK2-let-7 4x (column 1) or psiCHECK2-miR-20 (column 2), together with 48 nM of let-7. RNA levels (A) and luciferase activities (B) were determined 18 hr later. Numbers are mean ± SD (n = 3); **p < 0.01. See also Figure S1F.

(C and D) PA-1 cells were induced to express endogenous H19, followed by siRNA transfection. RNA (C) and protein (D) levels were measured 72 hr later. Numbers are mean ± SD (n = 3); *p < 0.05. See also Figures S3B and S3C.

(E) Bioinformatics predicted let-7 binding sites at three distinct positions in mouse H19. The nucleotides deleted in psiCHECK2-mH19D are marked in blue. See also Figures S4A–S4D.

(F) Luciferase assay results. Numbers are mean ± SD (n = 3).

experimental conditions used (see below), consistent with context-dependent miRNA effects (Ebert and Sharp, 2012; Mukherji et al., 2011). Together, these results suggest that ectopically expressed H19 inhibits endogenous let-7 function, leading to derepression of Dicer and Hmga2. In H19-expressing cells, the levels of the seven let-7 subtypes predicted to bind H19 were not significantly changed (Figure 4C).

To confirm that the observed effects were indeed due to impaired let-7 function, transfection experiments using iLet-7 (or iCon as a negative control) were performed. As expected, increased protein levels of both DICER and HMGA2 were observed in iLet-7-treated versus iCon-treated HEK 293 cells (Figure 4D, left panel, compare lane 2 to lane 1 in the top 2 blots). Further, when pH19mut, in which all four let-7 binding sites were inactivated, was used, derepression of Dicer and Hmga2 was not observed (Figure 4D, right panel, compare lane 2 to lane 1 in the top 2 blots), despite the fact that the mutant H19 was expressed at a level comparable to that of wild-type H19 (Figure S1B, compare the second column to the left and the last column). Again, the mRNA levels of Dicer and Hmga2 were not affected (Figures 4E and 4F), consistent with previous reports of translational repression without RNA destabilization (Filipowicz et al., 2008; Izaurralde, 2012) and context-dependent miRNA effects (Ebert and Sharp, 2012; Mukherji et al., 2011). These data suggest that the predicted let-7 binding sites in H19 are required for derepression of endogenous targets. Finally, derepression of DICER and HMGA2 in response to ectopic H19 expression was also observed when primary cultures of human umbilical vein endothelial cells (HUVECs) were tested (Figures S1C–S1E). Taken together, these results strongly suggest that derepression of endogenous let-7 targets Dicer and Hmga2 was due to a direct sponge effect of H19.

Next, we asked whether downregulating endogenous H19 would promote let-7 function. We first carried out reporter gene assays in PA-1 cells. PA-1 cells were induced to differentiate by retinoic acid (RA), followed by transfection of small interfering RNAs (siRNAs) specific for human H19 (siH19) or control siRNA (siCon). During differentiation, endogenous H19 typically rises to a level similar to that of beta-tubulin mRNA (Figure S1B, second column from right, red bar versus blue bar). Approximately 48 hr after the induction, the cells were transfected with reporter psiCHECK2-let-7 4x or psiCHECK-miR-20 (as a negative control), together with let-7 miRNA, and luciferase activities were measured 18 hr later. The levels of both endogenous let-7 and miR-20 were not affected by H19 downregulation (Figure S1F). As shown in Figure 5A, an ~95% knockdown of H19

48 hr following transfection with siH19 was observed (left column, red bar versus blue bar), while beta-actin mRNA was not affected (right column). Importantly, H19 knockdown was accompanied by an ~50% decrease in the Rluc activity of psiCHECK2-let-7 4x as compared to that of siCon-transfected cells (Figure 5B, column 1, red bar versus blue bar). In contrast, no Rluc activity change was observed with psiCHECK2-miR-20 (column 2, red bar versus blue bar), suggesting that H19 knockdown enables exogenously introduced let-7 to more effectively repress psiCHECK2-let-7 4x. Next, we asked whether H19 knockdown would activate endogenous let-7, using DICER as a read-out. Thus, H19 was downregulated in PA-1 cells using siH19 (or siH19b targeted to a different region of H19). Decreased DICER expression was observed when siH19 (Figures 5C and 5D) (or siH19b, Figures S3B and S3C) was used. Together, these results strongly point to the notion that H19 knockdown desequesters let-7, leading to heightened let-7 function.

Let-7 Regulation by H19 Is Conserved in Human and Mouse

To address whether the modulation of let-7 by H19 is evolutionarily conserved, bioinformatic analyses were performed, and putative let-7 binding sites in H19 were identified in other mammals, including mice (Figure 5E), rats, monkeys, chimpanzees, and bovine subjects (Figures S4A–S4D). A segment from mouse H19 containing binding sites for both let-7g and let-7e was inserted into the reporter to create psiCHECK2-mH19 and tested. Let-7e and let-7g, transfected either singly or in combination, inhibited Rluc activity in a dose-dependent fashion (Figure 5F, columns 1–3 from left). When a mutant reporter (psiCHECK2-mH19D) missing the sequences complementary to the seed region of both let-7e and let-7g was tested, a dose-dependent inhibition was not observed (Figure 5F, column 4). No dose-dependent inhibition was observed when miR-16-1 was tested on psiCHECK2-mH19 (Figure 5F, column 5). Together, these results suggest that the predicted let-7-binding sites in the mouse H19 are likely functional.

H19 Depletion Causes Accelerated Muscle Differentiation

To demonstrate that H19 regulation of let-7 is physiologically relevant, we turned to the mouse myogenic C2C12 cell line. Consistent with previous reports (Davis et al., 1987; Milligan et al., 2000), H19 expression was strongly induced during myoblast differentiation, beginning at day 1, peaking at day 3, and declining by day 4 of differentiation (Figure 6A, blue curve). A concomitant induction in let-7 was also observed (red curve). Since high let-7 levels are generally associated with increased differentiated states (Roush and Slack, 2008), we hypothesized that H19 might serve to inhibit let-7 activity, thereby preventing precocious differentiation. If this were the case, we would expect to see let-7 targets become downregulated as a result of H19 depletion. Thus, we transfected siRNA specific for mouse H19 (simH19) or control siRNA (siCon) into day 1 differentiating C2C12 myoblasts. RNAs were harvested 40 hr later and subjected to microarray experiments. We analyzed microarray data (Table S2) using SylArray, a web-server implementation of the Sylamer algorithm that uses the hypergeometric p values to measure significance of motif enrichment in the 3′ UTRs of ranked gene sets. Results are consistent with sponge effects by H19 on let-7 (Figures S5A and S5B). Our qPCR analysis on several known let-7 targets (Forman et al., 2008; Frost and Olson, 2011; Lee and Dutta, 2007; Tokumaru et al., 2008; Zhu et al., 2011) showed decreased levels of these targets in either simH19- or let-7-transfected cells (Figure 6B, compare green or purple bars to blue bars in the second through fifth columns from left). The specificity of simH19 was confirmed by experiments using a second siRNA targeted to another region of mouse H19 (Figure S6). It is notable that in differentiating mouse myoblasts, the mRNA levels of let-7 targets Dicer and Hmga2 decreased in response to increased let-7 function, a phenomenon that was not observed in proliferating HEK 293 cells (Figure 4) or HUVECs (Figures S1C and S1D), consistent with context-dependent miRNA effects (Ebert and Sharp, 2012; Mukherji et al., 2011). We also noticed that let-7 overexpression led to decreased H19 expression (Figure 6B, left first column, compare purple bar to blue bar), suggesting possible miRNP-mediated degradation of H19.

Next, we asked whether H19 depletion would produce a phenotype that mimics let-7 overexpression. Thus, differentiating C2C12 myoblasts were transfected with siCon, simH19, or let-7, followed by the assessment of myogenic differentiation. Both H19 depletion and let-7 overexpression led to significantly increased expression of muscle differentiation markers myosin heavy chain and myogenin at day 4 of differentiation (Figure 6C, left panel, compare lanes 2 and 3 to lane 1 in the top and middle blots, and right panel, compare green and purple bars to blue bars), suggesting enhanced myogenesis. Consistent with this finding, we observed increased multinucleated myotube formation in simH19- and let-7-transfected myoblasts (Figure 6D, compare right two panels to the left). This was reflected quantitatively as an increase in the fusion index as compared with siCon-transfected myoblasts (Figure 6E). Together, these results underscore the physiological significance of the H19-let-7 interaction while uncovering a previously unexpected regulatory network involving the H19/let-7 axis in myogenic differentiation.

In search of potential downstream effectors of H19/let-7-mediated regulation during muscle differentiation, we focused our attention on insulin-like growth factors (IGF1 and IGF2), major regulators of pre- and postnatal muscle development and growth (Braun and Gautel, 2011; Chang, 2007). IGF1 and IGF2 act through the same receptor, IGF1R, to promote myogenesis (Braun and Gautel, 2011; Chang, 2007). As a potent autocrine and paracrine regulator whose expression is rapidly induced early during differentiation, IGF2 stimulates muscle differentiation both in vivo (Borensztein et al., 2013; Kalista et al., 2012; Merrick et al., 2007) and in vitro (Rosen et al., 1993; Stewart et al., 1996; Wilson et al., 2003; Yoshiko et al., 2002). Importantly, let-7 has been shown to be an indirect upstream regulator of *Igf2* expression (Jung et al., 2010; Lu et al., 2007; 2011). Indeed, a positive in vivo correlation of expression between let-7 and *Igf2* has been documented in both epithelial ovarian cancer and breast cancer (Lu et al., 2007; 2011). In addition, experiments using HeLa cells transfected with let-7 have

Please cite this article in press as: Kallen et al., The Imprinted H19 LncRNA Antagonizes Let-7 MicroRNAs, Molecular Cell (2013), http://dx.doi.org/10.1016/j.molcel.2013.08.027

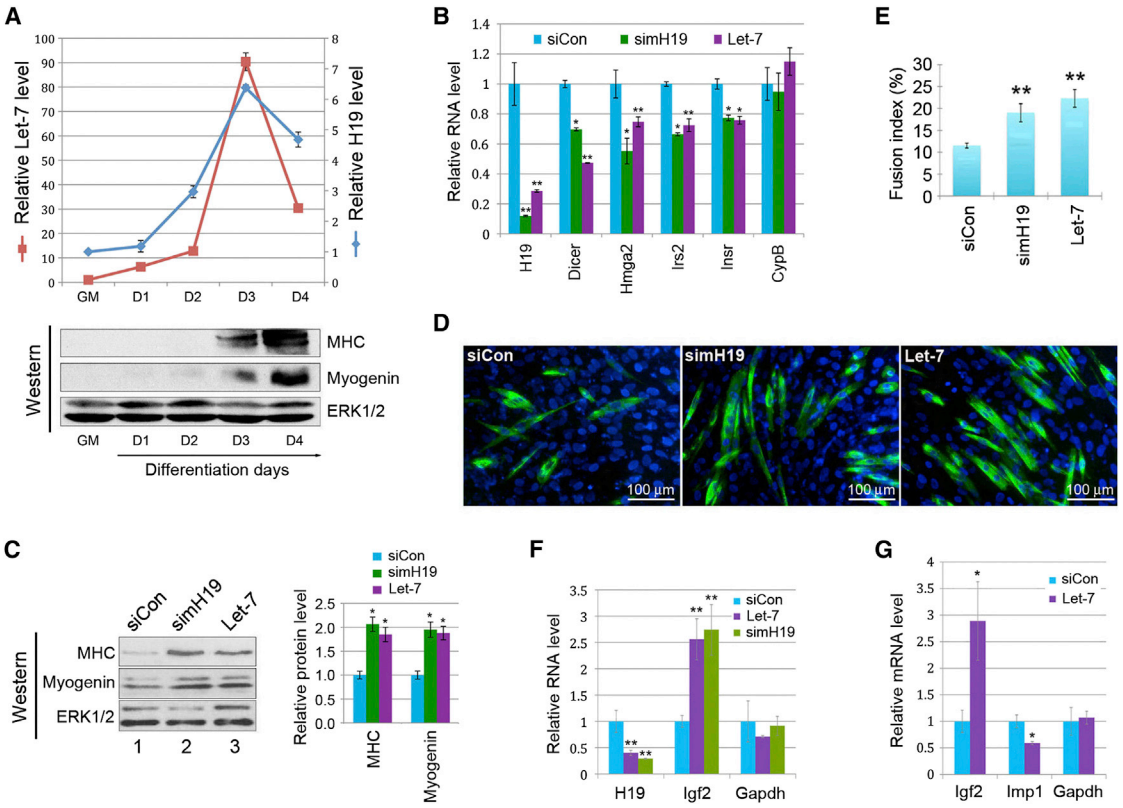

Figure 6. H19 Regulates Muscle Differentiation In Vitro

(A) C2C12 myoblasts were grown in growth medium (GM) or allowed to differentiate for 4 days. RNA and protein were harvested at the indicated time points and analyzed. Top: the expression profiles of H19 RNA and let-7a miRNA were analyzed by RT-qPCR, and results are presented with levels of GM set as 1. Numbers are mean ± SD (n = 3). Bottom: the expression profiles of muscle differentiation markers myosin heavy chain (MHC) and myogenin are shown by western blot analysis. ERK1 and ERK2 were used as loading controls.

(B) C2C12 myoblasts at day 1 differentiation were tranfected with siCon, simH19, or let-7. RNAs were harvested 40 hr later and analyzed by RT-qPCR. Relative RNA levels are presented after normalization against beta-tubulin mRNA. Numbers are mean ± SD (n = 3); *p < 0.05; **p < 0.01. See also Figures S5 and S6 and Table S2.

(C) Day 1 differentiating C2C12 myoblasts were transfected with siCon, simH19, or let-7. Proteins were harvested 3 days later and analyzed. Representative western blot gels are shown on the left. Bar graphs on the right show the quantitation of three separate western blot experiments. Numbers are mean ± SD (n = 3); *p < 0.05.

(D) MHC staining, representative of two separate experiments.

(E) Quantitation of myotube formation from (D). Numbers are mean ± SD (n = 5); **p < 0.01.

(F) RT-qPCR results of differentiating C2C12 myoblasts transfected with siCon, let-7, or simH19 as described in (B). Numbers are mean ± SD (n = 3); **p < 0.01.

(G) RT-qPCR results of proliferating C2C12 myoblasts transfected with siCon or let-7. Numbers are mean ± SD (n = 3); *p < 0.05.

demonstrated an upregulation of *Igf2* expression as a result of let-7 overexpression (Lu et al., 2011). This upregulation is thought to be mediated by the Igf2 mRNA-binding protein IMP1, which binds specifically to the 5′ UTR of Igf2 mRNA and inhibits its expression (Jung et al., 2010; Nielsen et al., 1999). Imp1 mRNA is a validated target of let-7 inhibition (Boyerinas et al., 2008; Ioannidis et al., 2005). Based on these previous studies, we hypothesized that *Igf2* might be a downstream effector of let-7-mediated regulation during myogenesis. In line with this view, we observed increased *Igf2* expression in differentiating myoblasts transfected with let-7 or simH19 (Figure 6F, middle column, compare purple or green bar with blue bar). To rule out myotube differentiation-dependent phenomena (as both H19 knockdown and let-7 overexpression accelerate myoblast differentiation [Figures 6C–6E], which can lead to increased *Igf2* expression), we performed let-7 transfection experiments in proliferating myoblasts that express low levels of H19. An increase in *Igf2* expression in response to let-7 overexpression was evident as well (Figure 6G, left column, compare purple bar with blue bar), suggesting that *Igf2* is a downstream effector of let-7, consistent with previous reports (Ioannidis et al., 2005; Jung et al., 2010; Lu et al., 2007; 2011). Importantly, let-7 overexpression led to decreased expression of Imp1 (Figure 6G, middle column, compare purple bar with blue bar), which might contribute, at least in part, to increased *Igf2* expression (Figure 6G, left column). In differentiating myoblasts, which express high levels of endogenous let-7 (Figure 6A, top panel), we did not detect Imp1 expression, consistent with Imp1 mRNA being a direct target of let-7 inhibition (Boyerinas et al., 2008; Ioannidis et al., 2005). Taken together, these results

suggest that *Igf2* is a downstream effector of H19/let-7-mediated regulation in myoblasts.

Given the wide range of putative targets of let-7 and the complex nature of signaling factors and pathways involved in pre- and postnatal muscle development (Braun and Gautel, 2011; Chang, 2007), we believe that other genes also function as downstream effectors of the H19/let-7-mediated regulation in muscle. Indeed, *Hmga2* knockout mice display skeletal muscle hypotrophy due to impaired myoblast proliferation, whereas *Dicer* knockout mice show decreased skeletal muscle mass with abnormal myofiber morphology, partly as a result of increased apoptosis in muscle cells (Li et al., 2012; O'Rourke et al., 2007). In line with a role in promoting myoblast proliferation or survival, both *Hmga2* and *Dicer* are highly expressed in proliferating myoblasts, and their expression declines upon differentiation (Li et al., 2012; O'Rourke et al., 2007; Sago et al., 2004). We find that both *Hmga2* and *Dicer* mRNA levels decrease in C2C12 myoblasts transfected with simH19 or let-7 (Figure 6B, second and third columns from left, compare green and purple bars with blue bars), consistent with *Hmga2* and *Dicer* being additional downstream effectors of H19/let-7-mediated regulation. Future studies dissecting detailed signal transduction pathways mediated by these effectors will be necessary to firmly establish this conclusion.

DISCUSSION

We find that the conserved, imprinted H19 lncRNA, which is highly expressed in the developing embryo and adult muscle, binds to let-7 and inhibits its function, acting as a molecular sponge. The physiological significance of this interaction is underscored using a myogenic differentiation model system where H19 depletion accelerates muscle differentiation, a phenotype recapitulated by let-7 overexpression. It has long been known that cellular miRNA abundance could be titrated for regulatory effect using artificial transcripts (miRNA sponges) that contain tandem repeats of miRNA-binding sites (Ebert and Sharp, 2010). Recently, a new class of endogenously expressed noncoding RNAs, called circular RNAs, has been demonstrated to act as potent miRNA sponges (Hansen et al., 2013; Memczak et al., 2013). In addition, mRNAs, transcribed pseudogenes, and other lncRNAs may function as miRNA sponges (Cesana et al., 2011; Poliseno et al., 2010; Tay et al., 2011). We find that H19, a developmentally regulated and abundantly expressed lncRNA, is a natural sponge for let-7.

Although the let-7-binding sites on H19 that we identify appear to be weak and not significantly conserved (as predicted by the currently available algorithms), they do in fact show appreciable levels of sponge effects using both reporter and endogenous genes as readouts under different conditions as well as in different cell types derived from different species. In addition, our crosslinking affinity purification experiments demonstrating an in vivo physical interaction between H19 and let-7 provide further support for H19's sponge activity. Importantly, our results are consistent with data from genetic testing (Didiano and Hobert, 2006), mammalian studies (Lal et al., 2009; Tay et al., 2008), and high-throughput RIP-Chip and CLIP studies (Chi et al., 2009; Hafner et al., 2010; Landthaler et al., 2008; Loeb et al., 2012). A comprehensive CLIP data analysis strongly suggests a substantial involvement of noncanonical sites in gene regulation (Liu et al., 2013). For example, lin-41, the first known target for let-7, only has two noncanonical sites (Vella et al., 2004). Among genetically identified let-7 targets in worms, 40% lack conserved binding sites (Hammell, 2010). Work from David Bartel's group suggests that a large fraction of nonconserved seed sites can be functional and some might represent important species-specific repression (Bartel, 2009). Thus, our findings reported here add to both the growing list of functional noncanonical sites and the list of nonconserved seed sites.

In addition to contributing to expansion of the repertoire of endogenous miRNA sponges, the significance of our findings is severalfold. First, high levels of H19 expression have been detected in fetal skeletal and cardiac muscle, in addition to fetal liver, yet the physiological significance of this expression is unknown (Gabory et al., 2010). Our results suggest that H19 likely plays a role in controlling timing of muscle differentiation in vivo by modulating the action of let-7. Recently, a muscle-specific lncRNA, called Linc-MD1, was reported to regulate myoblast differentiation by acting as a sponge for miR-133 and miR-135 (Cesana et al., 2011). Whether there is any crosstalk between the pathways regulated by these two lncRNAs remains to be investigated.

Second, given the abundant and broad expression pattern of H19 during embryogenesis, and given that the expression of both H19 and let-7 is developmentally regulated in a cell- and tissue-specific manner (Büssing et al., 2008; Gabory et al., 2010), we postulate that the H19/let-7 regulation may also contribute to other developmental processes. For example, *H19* deletion mice (*H19Δ3*) display an increase in both prenatal and postnatal growth compared to WT littermates, which is accompanied by an overexpression of *Igf2* and several other genes of the IGN involved in embryonic development and growth (Gabory et al., 2009). Remarkably, when an H19 transgene expressed from a site outside of the *H19-Igf2* locus was introduced back to the *H19* deletion animals, the overgrowth phenotype, together with the IGN gene overexpression, was restored to the WT level (Gabory et al., 2009). While a *cis*-acting effect of the transgenic H19 expression has been ruled out (Gabory et al., 2009), a transcriptional and/or posttranscriptional regulation of *Igf2* and other IGN genes by H19 lncRNA in contributing to the in vivo growth regulation remains possible. This is suggested by the notions that there exists a positive correlation of expression between let-7 and *Igf2* both in vivo (Lu et al., 2007; Lu et al., 2011) and in vitro (Figures 6F and 6G; Lu et al., 2011) and that downregulation of H19 increases *Igf2* expression (Figure 6F) and phenocopies let-7 overexpression (Figures 6D and 6E). It is therefore tempting to speculate that *H19Δ3* mice may have heightened let-7 activity, which in turn leads to increased *Igf2* expression, thereby contributing to the overgrowth phenotype.

Third, a high level of H19 expression persists in adult skeletal muscle (Gabory et al., 2010; Onyango and Feinberg, 2011). Because let-7 has been implicated in regulating glucose metabolism in muscle (Frost and Olson, 2011; Zhu et al., 2011), we speculate that H19 may modulate let-7 action in this organ, thereby contributing to glucose metabolism regulation. Fourth,

H19 contains putative binding sites for additional miRNAs (Table S1), suggesting that H19 may also regulate other miRNAs, perhaps in a tissue cell and developmental stage-dependent manner. It seems clear that H19 is likely to have role(s) in gene regulation beyond those of titrating let-7 and serving as a reservoir for miR-675.

EXPERIMENTAL PROCEDURES

Bioinformatic Analysis

miRNA-binding sites on H19 were predicted using a web-based program RNAhybrid (Rehmsmeier et al., 2004). To examine the evolutionary conservation of the binding sites in human H19 lncRNA, we used conversation scores for each nucleotide of H19 lncRNA. For the NCBI human H19 lncRNA sequence (NR_002196, build 37.3), the nucleotide-specific conservation score files were downloaded from UCSC genome browser (http://genome.ucsc.edu/). These files were generated by the phastCons program (Siepel et al., 2005) through multiple-sequence alignments of 33 mammalian genomes to the human genome (hg19). For Sylamer analysis, we used the SylArray program (http://bioinformatics.oxfordjournals.org/content/early/2010/09/24/bioinformatics.btq545.full.pdf). See also Supplemental Experimental Procedures.

Luciferase Assays, Immunoprecipitation, Western Blot, and RT-qPCR

These were carried out as previously described (Qiu et al., 2010). See also Supplemental Experimental Procedures.

In Vivo Formaldehyde Crosslinking and Affinity Purification

These were carried out as previously described (Vasudevan et al., 2007), with modifications. See also Supplemental Experimental Procedures.

C2C12 Myotube Derivation, Immunostaining, and Fusion Index

See Supplemental Experimental Procedures for detailed descriptions.

Microarray Experiments

Total RNAs were extracted from siRNA-transfected C2C12 myotubes. Hybridization and signal acquisition of the GeneChip Mouse Exon 1.0 ST Array (Affymetrix) containing a total of 29,000 gene transcripts was performed. Each array experiment was performed in triplicate. The signal intensities were normalized by the robust multiarray average (RMA) method using the Expression Console 1.1.2 (Affymetrix).

Statistical Analysis

All data are presented as mean ± SD. Data were analyzed using two-tailed Student's t test. p values at 0.05 or less were considered significant.

ACCESSION NUMBERS

The accession number for the microarray data reported in this paper is GSE49539.

SUPPLEMENTAL INFORMATION

Supplemental Information includes Supplemental Experimental Procedures, six figures, and two tables and can be found with this article online at http://dx.doi.org/10.1016/j.molcel.2013.08.027.

ACKNOWLEDGMENTS

We thank Wei Ma for helping with cloning and western blot analysis, Seth Guller for human term placental complementary DNA (cDNA), Gerald Shulman for mouse muscle samples, Yukihide Tomari for psiCHECK2-let-7 4x, Kunhua Chen (ExonBIO) for site-directed mutagenesis of full-length human H19, and the Computational Molecular Biology and Statistics Core at the Wadsworth Center for supporting computing resources. This work was supported by the following: CT Innovations Inc. grant 09SCAYALE14 and Albert McKern Scholar Award 1063338 to Y.H., Bennack-Polan Foundation R11756 to A.N.K., National Science Foundation grant DBI-0650991 to Y.D., and National Institutes of Health grant GM099811 to Y.D. and grant GM099801 to A.M.B.

Received: May 16, 2012
Revised: May 22, 2013
Accepted: August 6, 2013
Published: September 19, 2013

REFERENCES

Bartel, D.P. (2009). MicroRNAs: target recognition and regulatory functions. Cell *136*, 215–233.

Borensztein, M., Monnier, P., Court, F., Louault, Y., Ripoche, M.A., Tiret, L., Yao, Z., Tapscott, S.J., Forné, T., Montarras, D., and Dandolo, L. (2013). Myod and H19-Igf2 locus interactions are required for diaphragm formation in the mouse. Development *140*, 1231–1239.

Boyerinas, B., Park, S.M., Shomron, N., Hedegaard, M.M., Vinther, J., Andersen, J.S., Feig, C., Xu, J., Burge, C.B., and Peter, M.E. (2008). Identification of let-7-regulated oncofetal genes. Cancer Res. *68*, 2587–2591.

Brannan, C.I., Dees, E.C., Ingram, R.S., and Tilghman, S.M. (1990). The product of the H19 gene may function as an RNA. Mol. Cell. Biol. *10*, 28–36.

Braun, T., and Gautel, M. (2011). Transcriptional mechanisms regulating skeletal muscle differentiation, growth and homeostasis. Nat. Rev. Mol. Cell Biol. *12*, 349–361.

Büssing, I., Slack, F.J., and Grosshans, H. (2008). let-7 microRNAs in development, stem cells and cancer. Trends Mol. Med. *14*, 400–409.

Cesana, M., Cacchiarelli, D., Legnini, I., Santini, T., Sthandier, O., Chinappi, M., Tramontano, A., and Bozzoni, I. (2011). A long noncoding RNA controls muscle differentiation by functioning as a competing endogenous RNA. Cell *147*, 358–369.

Chang, K.C. (2007). Key signalling factors and pathways in the molecular determination of skeletal muscle phenotype. Animal *1*, 681–698.

Chi, S.W., Zang, J.B., Mele, A., and Darnell, R.B. (2009). Argonaute HITS-CLIP decodes microRNA-mRNA interaction maps. Nature *460*, 479–486.

Davis, R.L., Weintraub, H., and Lassar, A.B. (1987). Expression of a single transfected cDNA converts fibroblasts to myoblasts. Cell *51*, 987–1000.

Didiano, D., and Hobert, O. (2006). Perfect seed pairing is not a generally reliable predictor for miRNA-target interactions. Nat. Struct. Mol. Biol. *13*, 849–851.

Ebert, M.S., and Sharp, P.A. (2010). Emerging roles for natural microRNA sponges. Curr. Biol. *20*, R858–R861.

Ebert, M.S., and Sharp, P.A. (2012). Roles for microRNAs in conferring robustness to biological processes. Cell *149*, 515–524.

Fabian, M.R., and Sonenberg, N. (2012). The mechanics of miRNA-mediated gene silencing: a look under the hood of miRISC. Nat. Struct. Mol. Biol. *19*, 586–593.

Filipowicz, W., Bhattacharyya, S.N., and Sonenberg, N. (2008). Mechanisms of post-transcriptional regulation by microRNAs: are the answers in sight? Nat. Rev. Genet. *9*, 102–114.

Forman, J.J., Legesse-Miller, A., and Coller, H.A. (2008). A search for conserved sequences in coding regions reveals that the let-7 microRNA targets Dicer within its coding sequence. Proc. Natl. Acad. Sci. USA *105*, 14879–14884.

Frost, R.J., and Olson, E.N. (2011). Control of glucose homeostasis and insulin sensitivity by the Let-7 family of microRNAs. Proc. Natl. Acad. Sci. USA *108*, 21075–21080.

Gabory, A., Ripoche, M.A., Le Digarcher, A., Watrin, F., Ziyyat, A., Forné, T., Jammes, H., Ainscough, J.F., Surani, M.A., Journot, L., and Dandolo, L. (2009). H19 acts as a trans regulator of the imprinted gene network controlling growth in mice. Development *136*, 3413–3421.

Gabory, A., Jammes, H., and Dandolo, L. (2010). The H19 locus: role of an imprinted non-coding RNA in growth and development. Bioessays *32*, 473–480.

Hafner, M., Landthaler, M., Burger, L., Khorshid, M., Hausser, J., Berninger, P., Rothballer, A., Ascano, M., Jr., Jungkamp, A.C., Munschauer, M., et al. (2010). Transcriptome-wide identification of RNA-binding protein and microRNA target sites by PAR-CLIP. Cell *141*, 129–141.

Hammell, M. (2010). Computational methods to identify miRNA targets. Semin. Cell Dev. Biol. *21*, 738–744.

Hansen, T.B., Jensen, T.I., Clausen, B.H., Bramsen, J.B., Finsen, B., Damgaard, C.K., and Kjems, J. (2013). Natural RNA circles function as efficient microRNA sponges. Nature *495*, 384–388.

Ioannidis, P., Mahaira, L.G., Perez, S.A., Gritzapis, A.D., Sotiropoulou, P.A., Kavalakis, G.J., Antsaklis, A.I., Baxevanis, C.N., and Papamichail, M. (2005). CRD-BP/IMP1 expression characterizes cord blood CD34+ stem cells and affects c-myc and IGF-II expression in MCF-7 cancer cells. J. Biol. Chem. *280*, 20086–20093.

Iwasaki, S., Kawamata, T., and Tomari, Y. (2009). Drosophila argonaute1 and argonaute2 employ distinct mechanisms for translational repression. Mol. Cell *34*, 58–67.

Izaurralde, E. (2012). Elucidating the temporal order of silencing. EMBO Rep. *13*, 662–663.

Jung, Y.H., Gupta, M.K., Shin, J.Y., Uhm, S.J., and Lee, H.T. (2010). MicroRNA signature in testes-derived male germ-line stem cells. Mol. Hum. Reprod. *16*, 804–810.

Kalista, S., Schakman, O., Gilson, H., Lause, P., Demeulder, B., Bertrand, L., Pende, M., and Thissen, J.P. (2012). The type 1 insulin-like growth factor receptor (IGF-IR) pathway is mandatory for the follistatin-induced skeletal muscle hypertrophy. Endocrinology *153*, 241–253.

Keniry, A., Oxley, D., Monnier, P., Kyba, M., Dandolo, L., Smits, G., and Reik, W. (2012). The H19 lincRNA is a developmental reservoir of miR-675 that suppresses growth and Igf1r. Nat. Cell Biol. *14*, 659–665.

Lal, A., Navarro, F., Maher, C.A., Maliszewski, L.E., Yan, N., O'Day, E., Chowdhury, D., Dykxhoorn, D.M., Tsai, P., Hofmann, O., et al. (2009). miR-24 Inhibits cell proliferation by targeting E2F2, MYC, and other cell-cycle genes via binding to "seedless" 3'UTR microRNA recognition elements. Mol. Cell *35*, 610–625.

Landthaler, M., Gaidatzis, D., Rothballer, A., Chen, P.Y., Soll, S.J., Dinic, L., Ojo, T., Hafner, M., Zavolan, M., and Tuschl, T. (2008). Molecular characterization of human Argonaute-containing ribonucleoprotein complexes and their bound target mRNAs. RNA *14*, 2580–2596.

Lee, Y.S., and Dutta, A. (2007). The tumor suppressor microRNA let-7 represses the HMGA2 oncogene. Genes Dev. *21*, 1025–1030.

Li, Z., Gilbert, J.A., Zhang, Y., Zhang, M., Qiu, Q., Ramanujan, K., Shavlakadze, T., Eash, J.K., Scaramozza, A., Goddeeris, M.M., et al. (2012). An HMGA2-IGF2BP2 axis regulates myoblast proliferation and myogenesis. Dev. Cell *23*, 1176–1188.

Liu, C., Mallick, B., Long, D., Rennie, W.A., Wolenc, A., Carmack, C.S., and Ding, Y. (2013). CLIP-based prediction of mammalian microRNA binding sites. Nucleic Acids Res. *41*, e138, http://dx.doi.org/10.1093/nar/gkt1435.

Loeb, G.B., Khan, A.A., Canner, D., Hiatt, J.B., Shendure, J., Darnell, R.B., Leslie, C.S., and Rudensky, A.Y. (2012). Transcriptome-wide miR-155 binding map reveals widespread noncanonical microRNA targeting. Mol. Cell *48*, 760–770.

Lu, L., Katsaros, D., de la Longrais, I.A., Sochirca, O., and Yu, H. (2007). Hypermethylation of let-7a-3 in epithelial ovarian cancer is associated with low insulin-like growth factor-II expression and favorable prognosis. Cancer Res. *67*, 10117–10122.

Lu, L., Katsaros, D., Zhu, Y., Hoffman, A., Luca, S., Marion, C.E., Mu, L., Risch, H., and Yu, H. (2011). Let-7a regulation of insulin-like growth factors in breast cancer. Breast Cancer Res. Treat. *126*, 687–694.

Matouk, I.J., DeGroot, N., Mezan, S., Ayesh, S., Abu-lail, R., Hochberg, A., and Galun, E. (2007). The H19 non-coding RNA is essential for human tumor growth. PLoS ONE *2*, e845.

McKarney, L.A., Overall, M.L., and Dziadek, M. (1996). Expression of H19 and Igf2 genes in uniparental mouse ES cells during in vitro and in vivo differentiation. Differentiation *60*, 75–86.

Memczak, S., Jens, M., Elefsinioti, A., Torti, F., Krueger, J., Rybak, A., Maier, L., Mackowiak, S.D., Gregersen, L.H., Munschauer, M., et al. (2013). Circular RNAs are a large class of animal RNAs with regulatory potency. Nature *495*, 333–338.

Merrick, D., Ting, T., Stadler, L.K., and Smith, J. (2007). A role for Insulin-like growth factor 2 in specification of the fast skeletal muscle fibre. BMC Dev. Biol. *7*, 65.

Milligan, L., Antoine, E., Bisbal, C., Weber, M., Brunel, C., Forné, T., and Cathala, G. (2000). H19 gene expression is up-regulated exclusively by stabilization of the RNA during muscle cell differentiation. Oncogene *19*, 5810–5816.

Mukherji, S., Ebert, M.S., Zheng, G.X., Tsang, J.S., Sharp, P.A., and van Oudenaarden, A. (2011). MicroRNAs can generate thresholds in target gene expression. Nat. Genet. *43*, 854–859.

Nielsen, J., Christiansen, J., Lykke-Andersen, J., Johnsen, A.H., Wewer, U.M., and Nielsen, F.C. (1999). A family of insulin-like growth factor II mRNA-binding proteins represses translation in late development. Mol. Cell. Biol. *19*, 1262–1270.

O'Rourke, J.R., Georges, S.A., Seay, H.R., Tapscott, S.J., McManus, M.T., Goldhamer, D.J., Swanson, M.S., and Harfe, B.D. (2007). Essential role for Dicer during skeletal muscle development. Dev. Biol. *311*, 359–368.

Onyango, P., and Feinberg, A.P. (2011). A nucleolar protein, H19 opposite tumor suppressor (HOTS), is a tumor growth inhibitor encoded by a human imprinted H19 antisense transcript. Proc. Natl. Acad. Sci. USA *108*, 16759–16764.

Poliseno, L., Salmena, L., Zhang, J., Carver, B., Haveman, W.J., and Pandolfi, P.P. (2010). A coding-independent function of gene and pseudogene mRNAs regulates tumour biology. Nature *465*, 1033–1038.

Qiu, C., Ma, Y., Wang, J., Peng, S., and Huang, Y. (2010). Lin28-mediated post-transcriptional regulation of Oct4 expression in human embryonic stem cells. Nucleic Acids Res. *38*, 1240–1248.

Rehmsmeier, M., Steffen, P., Hochsmann, M., and Giegerich, R. (2004). Fast and effective prediction of microRNA/target duplexes. RNA *10*, 1507–1517.

Rosen, K.M., Wentworth, B.M., Rosenthal, N., and Villa-Komaroff, L. (1993). Specific, temporally regulated expression of the insulin-like growth factor II gene during muscle cell differentiation. Endocrinology *133*, 474–481.

Roush, S., and Slack, F.J. (2008). The let-7 family of microRNAs. Trends Cell Biol. *18*, 505–516.

Sago, N., Omi, K., Tamura, Y., Kunugi, H., Toyo-oka, T., Tokunaga, K., and Hohjoh, H. (2004). RNAi induction and activation in mammalian muscle cells where Dicer and eIF2C translation initiation factors are barely expressed. Biochem. Biophys. Res. Commun. *319*, 50–57.

Salmena, L., Poliseno, L., Tay, Y., Kats, L., and Pandolfi, P.P. (2011). A ceRNA hypothesis: the Rosetta Stone of a hidden RNA language? Cell *146*, 353–358.

Siepel, A., Bejerano, G., Pedersen, J.S., Hinrichs, A.S., Hou, M., Rosenbloom, K., Clawson, H., Spieth, J., Hillier, L.W., Richards, S., et al. (2005). Evolutionarily conserved elements in vertebrate, insect, worm, and yeast genomes. Genome Res. *15*, 1034–1050.

Stewart, C.E., James, P.L., Fant, M.E., and Rotwein, P. (1996). Overexpression of insulin-like growth factor-II induces accelerated myoblast differentiation. J. Cell. Physiol. *169*, 23–32.

Tay, Y., Zhang, J., Thomson, A.M., Lim, B., and Rigoutsos, I. (2008). MicroRNAs to Nanog, Oct4 and Sox2 coding regions modulate embryonic stem cell differentiation. Nature *455*, 1124–1128.

Tay, Y., Kats, L., Salmena, L., Weiss, D., Tan, S.M., Ala, U., Karreth, F., Poliseno, L., Provero, P., Di Cunto, F., et al. (2011). Coding-independent

regulation of the tumor suppressor PTEN by competing endogenous mRNAs. Cell *147*, 344–357.

Tokumaru, S., Suzuki, M., Yamada, H., Nagino, M., and Takahashi, T. (2008). let-7 regulates Dicer expression and constitutes a negative feedback loop. Carcinogenesis *29*, 2073–2077.

Varrault, A., Gueydan, C., Delalbre, A., Bellmann, A., Houssami, S., Aknin, C., Severac, D., Chotard, L., Kahli, M., Le Digarcher, A., et al. (2006). Zac1 regulates an imprinted gene network critically involved in the control of embryonic growth. Dev. Cell *11*, 711–722.

Vasudevan, S., Tong, Y., and Steitz, J.A. (2007). Switching from repression to activation: microRNAs can up-regulate translation. Science *318*, 1931–1934.

Vella, M.C., Choi, E.Y., Lin, S.Y., Reinert, K., and Slack, F.J. (2004). The C. elegans microRNA let-7 binds to imperfect let-7 complementary sites from the lin-41 3'UTR. Genes Dev. *18*, 132–137.

Wilson, E.M., Hsieh, M.M., and Rotwein, P. (2003). Autocrine growth factor signaling by insulin-like growth factor-II mediates MyoD-stimulated myocyte maturation. J. Biol. Chem. *278*, 41109–41113.

Yoshiko, Y., Hirao, K., and Maeda, N. (2002). Differentiation in C(2)C(12) myoblasts depends on the expression of endogenous IGFs and not serum depletion. Am. J. Physiol. Cell Physiol. *283*, C1278–C1286.

Yoshimizu, T., Miroglio, A., Ripoche, M.A., Gabory, A., Vernucci, M., Riccio, A., Colnot, S., Godard, C., Terris, B., Jammes, H., and Dandolo, L. (2008). The H19 locus acts in vivo as a tumor suppressor. Proc. Natl. Acad. Sci. USA *105*, 12417–12422.

Zhu, H., Shyh-Chang, N., Segrè, A.V., Shinoda, G., Shah, S.P., Einhorn, W.S., Takeuchi, A., Engreitz, J.M., Hagan, J.P., Kharas, M.G., et al.; DIAGRAM Consortium; MAGIC Investigators. (2011). The Lin28/let-7 axis regulates glucose metabolism. Cell *147*, 81–94.